
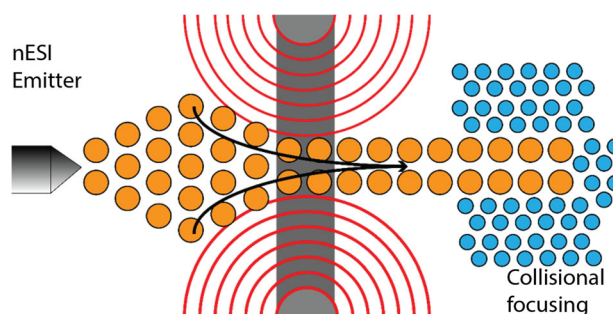


# Ion Manipulation in Open Air Using 3D-Printed Electrodes

Kiran Iyer,<sup>1</sup> Brett M. Marsh,<sup>1</sup> Grace O. Capek,<sup>1</sup> Robert L. Schrader,<sup>1</sup> Shane Tichy,<sup>2</sup>  
R. Graham Cooks<sup>1</sup> 

<sup>1</sup>Department of Chemistry, Purdue University, West Lafayette, IN 47907, USA

<sup>2</sup>Agilent Technologies, 5301 Stevens Creek Blvd, Santa Clara, CA 95051, USA



**Abstract.** Ambient ionization techniques provide a way to sample materials via creation of ions in the air. However, transferring and focusing of these ions is typically done in the reduced pressure environment of the mass spectrometer. Spray-based ambient ionization sources require relatively large distances between the source and mass spectrometer inlet for effective desolvation, resulting in a small fraction of the ions being collected. To increase the efficiency of ion trans-

fer from atmosphere to vacuum, 3D-printed focusing devices made of conductive carbon nanotube doped polymers have been designed and evaluated for ion focusing in air. Three main classes of electrodes are considered: (i) conic section electrodes (conical, ellipsoidal, and cylindrical), (ii) simple conductive and non-conductive apertures, and (iii) electrodes with complex geometries (straight, chicane, and curved). Simulations of ion trajectories performed using the statistical diffusion simulation (SDS) model in SIMION showed a measure of agreement with experiment. Cross-sectional images of ion beams were captured using an ion detecting charge-coupled device (IonCCD). After optimization, the best arrangements of electrodes were coupled to an Agilent Ultivo triple quadrupole to record mass spectra. Observations suggest that electrode geometry strongly influences ion trajectories in air. Non-conductive electrodes also assisted in focusing, due to charge buildup from ion deposition. We also observed minimal spreading of the ion packet after exiting the focusing electrodes indicating that atmospheric collisions do not reduce collimation of the beam. The study suggests that high pressures need not be viewed as a hindrance to ion transport, but as a potentially useful force.

**Keywords:** Ambient ionization, Additive manufacturing, Ion focusing, Triple quadrupole, Ion transmission

Received: 20 May 2019/Revised: 31 July 2019/Accepted: 2 August 2019/Published Online: 11 November 2019

Kiran Iyer and Brett M. Marsh contributed equally to this work.

Dedicated to Prof. Helmut Schwarz in admiration of the quality and quantity of his science

**Electronic supplementary material** The online version of this article (<https://doi.org/10.1007/s13361-019-02307-2>) contains supplementary material, which is available to authorized users.

Correspondence to: Shane Tichy; e-mail: shane\_tichy@agilent.com, R. Cooks; e-mail: cooks@purdue.edu

## Introduction

The ability to manipulate ions in the air is of great importance in mass spectrometry (MS) due to the widespread adoption of electrospray ionization (ESI) [1] and of ambient ionization techniques [2–6] as the ionization methods of choice for many users. Typically, ions are generated at atmospheric pressure and allowed to propagate into the vacuum region of the mass spectrometer where they are focused and analyzed. However, the efficiency of ion transmission is often poor due to the spreading of ions from the spray and the small orifices used in mass spectrometers, leading to rejection of most of the ion signal [7, 8]. Additionally, in order to aid desolvation and so produce gas-phase ions, ion sources need to operate either at significant distances from the instrument, or they must be

operated with a heated sheath gas [9]. While ion funnels may assist in solving this problem, they can only operate under reduced pressure and their operation requires relatively complex radio frequency (RF) voltages [10]. Thus far little has been done to create avenues for manipulating ions under ambient conditions (i.e., in the open air) to improve their transmission to the mass spectrometer.

Ion optical simulations under reduced pressure continue to be a uniquely valuable resource in the development of unique MS instrumentation [11, 12]. It is less common to attempt to use ion-optical simulations to investigate ambient pressure ion manipulation or ion focusing. An early observation of this type was made when performing ambient ion soft-landing experiments, where it was observed that after passing through an aperture, ions became focused into a spot much smaller than the aperture [13]. This result was consistent with an earlier observation by Hayn and coworkers during the deposition of organic molecules at atmospheric pressure [14]. A similar effect was observed when placing a transmission electron microscopy (TEM) grid in front of an ESI source, the ion beam being focused by a factor of ten compared with the size of the TEM grid holes [15]. Experiments using ellipsoidally shaped electrodes as well as curved geometries [16, 17] indicated that ions could be transported over significant (> 1 cm) distances in the air while maintaining focus using only DC potentials. Despite this early work, many questions remain as to the mechanism of ion focusing in air, the usefulness of which is just beginning to be realized.

Presented here is a series of experiments utilizing 3D-printed focusing devices which seek to provide insight into the mechanism of ambient pressure focusing. Electrode designs were generated using AutoCAD software and then imported as stereolithography (.stl) files into Simplify 3D, a “slicing” program used to break up the model into “layers”. The layers are imported as gcode into the operating system of the 3D printer. Fused deposition modeling (FDM) was used to construct three sets of electrodes—(i) conical, ellipsoidal, and cylindrical electrodes (all conic section electrodes), (ii) both conductive and non-conductive simple aperture electrodes, and (iii) curved electrodes with complex geometries (straight, chicane, and curved). 3D-printing offered a quick and inexpensive way to construct and render various electrode designs [18]. Ion simulations were performed concurrently using the statistical diffusion model (SDS) in SIMION 8.1. To test the performance of the focusing devices, cross-sections of ion packets focused by the different electrodes were recorded using an IonCCD camera [19]. Additionally, the electrodes were coupled to an Agilent Ultivo Triple Quadrupole MS and mass spectrometric measurements were performed using a mixture of tetra alkyl ammonium (TAA) bromide salts.

## Experimental

### *Focusing Electrode Designs*

Three sets of devices were designed using AutoCAD software. The first set—conic section electrodes—is comprised of three

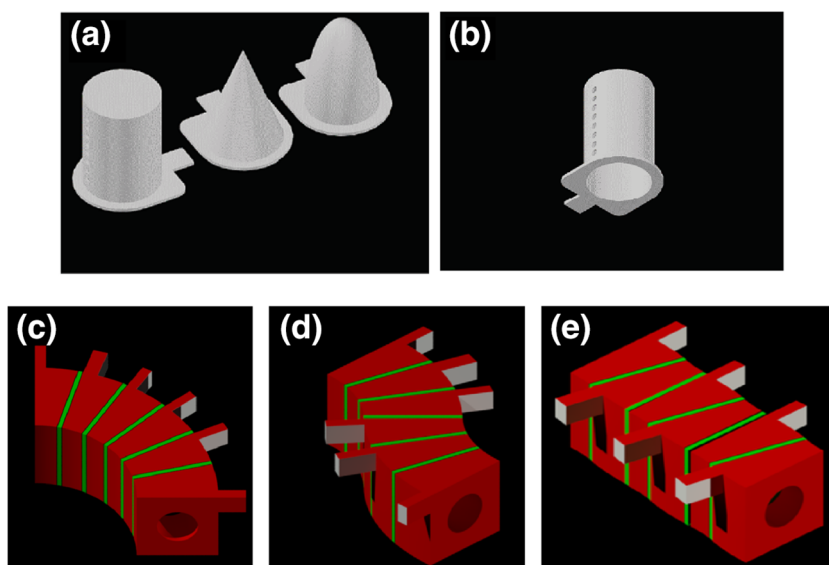
geometries, cylindrical, conical, and ellipsoidal. Each electrode has an opening of 30 mm, an internal length of 50 mm, and holes on one side spaced in 5-mm increments from the opening to the back of the object (Figure 1a, b). The second set of electrodes—the conductive and the non-conductive apertures (not shown in the figure) are simple 2D objects 3, 9, 12, and 15 mm in diameter. The six individual electrodes which comprise the complex geometry electrodes have a curvature of 15 degrees with 20-mm diameter openings (Figure 1c–e). To generate these electrode systems, the conic electrode components are arranged to give different geometries.

### *3D-Printing*

The conic section electrodes were printed at 265 °C using a modified Prusa i3 printer (Makerfarm, UT, USA) from polyethyleneterephthalate glycol (PETG) polymer-containing multiwalled carbon nanotubes (3DXTech, MI, USA). High extrusion temperatures are necessary as lower extrusion temperatures produce non-conducting electrodes. The print surface was covered in polyimide tape and heated to 70 °C to increase bed adhesion. The conductive apertures and complex geometry electrodes were printed using a Mendel Max 3 (Maker’s Tool Works, OK, USA) printer with carbon-doped conductive polylactic acid (PLA) filament (Proto-pasta, WA, USA). To check the conductivity of the printed electrodes, a voltage of 3 kV was applied to one end of the electrode, and the voltage at the other end was measured. All electrodes showed no measurable decrease in voltage across the object, indicating that they had adequate conductivity. Non-conductive apertures were printed using non-conductive PLA using a MendelMax 3 printer with extrusion temperature of 210 °C and heated glass bed at 50 °C with non-conductive PLA/polyhydroxyalkanoate (PHA) filament (ColorFabb, Belfeld, Netherlands).

### *IonCCD Current Measurements*

The cross-sections of the ion packets focused by the different electrodes were recorded using an IonCCD camera (OI Analytical, TX, USA) operated in air. The IonCCD consists of a detector array, composed of 2126 21- $\mu\text{m}$ -wide titanium nitride pixels, each 1.5 mm in height. The pixel separation is 3  $\mu\text{m}$ , giving an effective resolution of 24  $\mu\text{m}$  per pixel. Incoming ions are neutralized on the TiN pixels, giving rise to the current recorded by the IonCCD software. For experiments involving the conic section electrodes, the current was recorded over a time of 100 ms. For the aperture electrodes and the series electrodes, electrospray beam images were profiled by scanning the IonCCD in the horizontal dimension in 0.65-mm steps with the pixel row held constant in the vertical position. IonCCD images were processed by subtracting the signal with the electrospray off (background signal) from the IonCCD signal recorded with the electrospray on and focusing electrode operated. The intensity of features in the IonCCD spectrum is given in digital numbers (dN). Each dN unit corresponds to 100 elementary charges. Exact parameters for these experiments,



**Figure 1.** (a) Conic section electrodes (50-mm long) in cylindrical, conical, and ellipsoidal geometries. (b) Cylindrical electrode showing the holes on the side spaced 5 mm apart and having diameters of  $\sim 1$  mm to allow for the placement of a nanoelectrospray emitter. (c, d, e) curved, chicane, and straight complex electrodes (openings here are 20 mm)

including electrode and emitter voltages, are discussed in the results and discussion section.

### *SIMION Simulations*

Simulations of ion trajectories were performed using the statistical diffusion simulation (SDS) model in SIMION 8.1. Briefly, SDS is a computationally efficient method for simulation of collisions of ions with background gas. Diffusion of ions is simulated by random jumps of the ions at each time step. The jump distance is determined by collision statistics calculated for the ion. The SDS algorithm has been previously validated for simulations of atmospheric ion transport and ion mobility [20]. The simulations here only consider the ions as fully desolvated and do not consider the dynamic droplet evolution process which nESI sprays undergo after droplet creation.

### *Mass Spectrometry (MS)*

MS measurements were performed using an Agilent Ultivo triple quadrupole mass spectrometer. External nanoelectrospray ionization (nESI) was used to generate ions. A platinum wire served as the electrode. nESI emitters were pulled using borosilicate glass capillaries (0.86-mm ID, Sutter Instruments, CA, USA) using a micropipette tip puller (Model P-97, Sutter Instruments, CA, USA). The nESI tips had an outer diameter of  $\sim 5$   $\mu\text{m}$ . For nESI measurements, analyte solution was loaded into the pulled glass capillary using a gel loading tip (Bio-Rad, Hercules, CA). DC potentials were applied to the Pt wire using an external power supply. For nESI measurements, the source and electrodes (if any) were placed directly in front of the inlet of the MS and at a specific distance from it. The capillary in the source of the instrument was held at a positive set point of 100 V and the DC potential applied using an external power supply. For measurements using the nESI

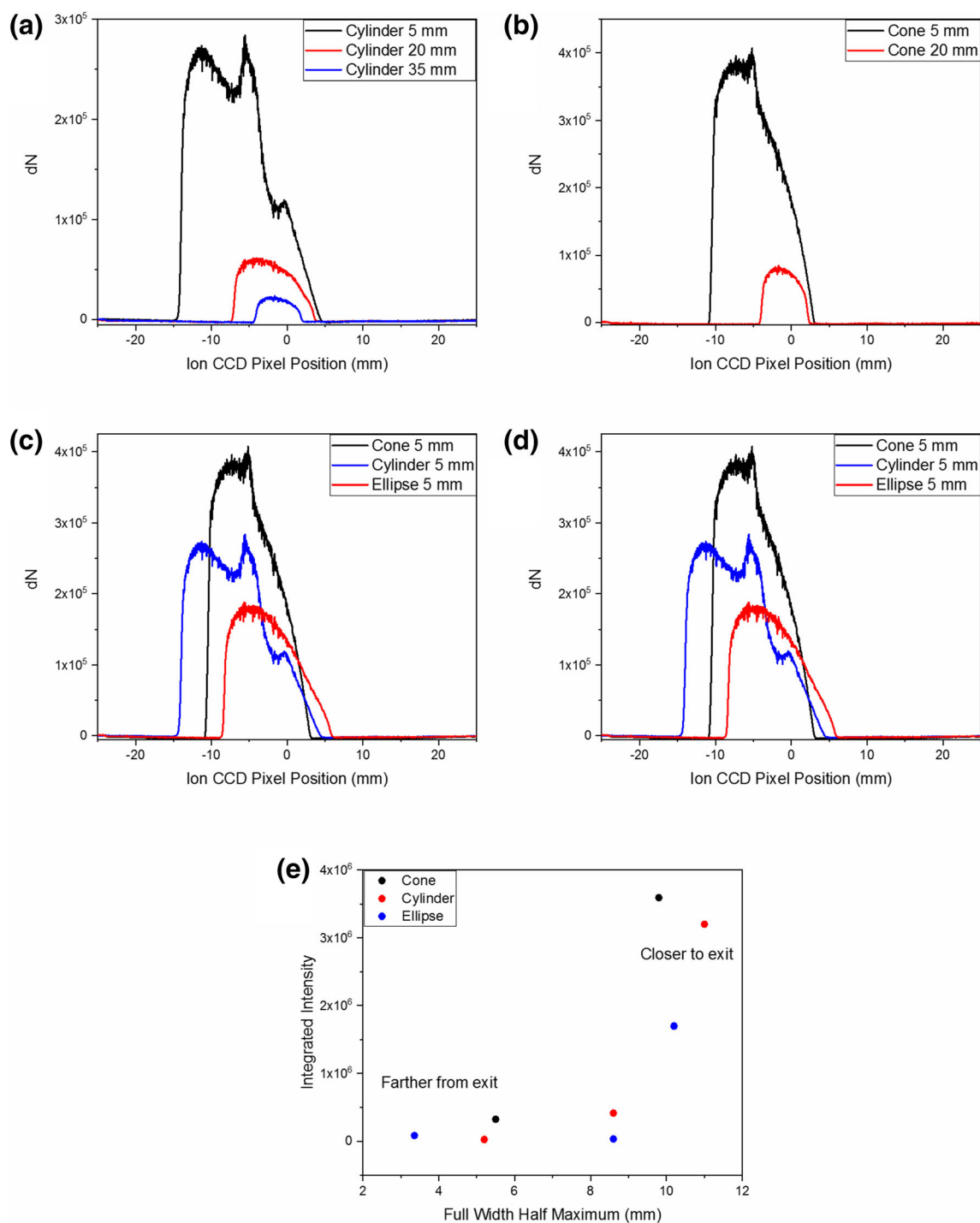
emitter alone, spectra were recorded at distances of 5 cm and 60 cm from the inlet. For measurements using the focusing electrodes, the nanospray emitter was placed orthogonally to the ion optical path of the instrument and inside the conic section focusing electrode using the holes on its side. The orthogonal orientation of the emitter in the electrode was chosen so as to decrease the flux of neutral species into the ion beam. For all measurements using the conductive electrodes, the nESI emitter was always held at a higher potential than the electrode. The entire electrode setup (supplemental Fig. S1) was placed in front of the MS inlet at different distances, and spectra were recorded using the same source conditions described above. Analyte used was a solution consisting of a mixture of tetraalkylammonium (TAA) bromide salts ( $\text{C}_2$ ,  $\text{C}_3$ ,  $\text{C}_4$ ,  $\text{C}_5$ ,  $\text{C}_6$ ,  $\text{C}_7$ ,  $\text{C}_8$ ) at 20  $\mu\text{M}$ .

## Results and Discussion

### *Conical Section Electrodes*

To understand how electrode geometry, and therefore the electric field, influences ion trajectories, a series of measurements was recorded with each set of electrodes using the IonCCD detector. The first set of measurements, performed using the electrodes of conical, ellipsoidal, and cylindrical profiles, examined how emitter position within the electrode influences the size and intensity of the exiting ion packet. For IonCCD measurements, the nESI emitter was held at 4.5 kV while the electrode was held at 3 kV. The IonCCD was held 15 mm away from the electrode exit for all three cases.

The resulting data (Figure 2) show two trends. First, in general, as the emitter is placed farther from the electrode exit, the peak recorded at the IonCCD becomes narrower. However,



**Figure 2.** Cross sectional beam images recorded with an IonCCD camera for the (a) conical, (b) cylindrical, and (c) ellipsoidal focusing electrodes. nESI sprayer was held at 4.5 kV while the focusing electrode was held at 3 kV. (d) Ion beam cross section at 5 mm for each electrode. (e) Summary of focusing data for each electrode and emitter distance recorded in these experiments

a significant decrease in the ion intensity was also observed. The difference in intensity is attributed to microdroplet evaporation throughout flight with scattering of the desolvated ions. Second, the conical electrode gives significantly better focusing than the ellipsoidal or cylindrical electrodes at a given distance. However, the cone displayed no measurable signal when the emitter was inserted into the 35 mm hole from the exit

(hole 7), which is attributed to the narrowness of the electrode at that location. Such effects are suggestive of a strong geometrical effect on the focusing observed. The asymmetry in the peaks is due to the nanospray emitter influencing the ion packet, as seen in ref. 16. The ion current, measured at the IonCCD as a function of peak full width half mass (FWHM) is shown for all measurements in Figure 2.

For MS measurements, the nESI emitter was held orthogonally to and just inside the focusing electrode using the holes on the side. Mass spectra were recorded at close distances (5 cm) and long distances (60 cm) with and without the focusing electrode. For all experiments, the nESI emitter was always held at a higher voltage than the focusing electrode. When the nESI emitter is placed orthogonally at a distance of 5 cm without the focusing electrode, the cations of all salts— $C_2$  to  $C_8$ —are observed in the spectrum, while at farther distances, only  $C_2$  to  $C_6$  salts are observed (Figure 3a). The voltage on the nESI emitter for these experiments was 2 kV. There is also a significant drop in the signal intensity as the nESI emitter is moved farther away. When the focusing electrode is introduced in the 60-cm experiment, higher mass TAAs are recovered, accompanied by an order of magnitude increase in intensity in signal as seen in Figure 3b. For these results, the nESI emitter was held at 3 kV while the focusing electrode was held at 2 kV. The resultant potential difference is 1 kV. We observed a proportional change in signal intensity when the potential difference was increased, attributed to the increase in kinetic energy that accompanies the increased voltage on the emitter. The increased transmission of high mass ions is also evidence of a long range effect resulting from ion focusing. In other words, ions which are focused in the electrode appear to maintain focus over the entire transmission distance, although some losses in intensity are observed. This effect is illustrated

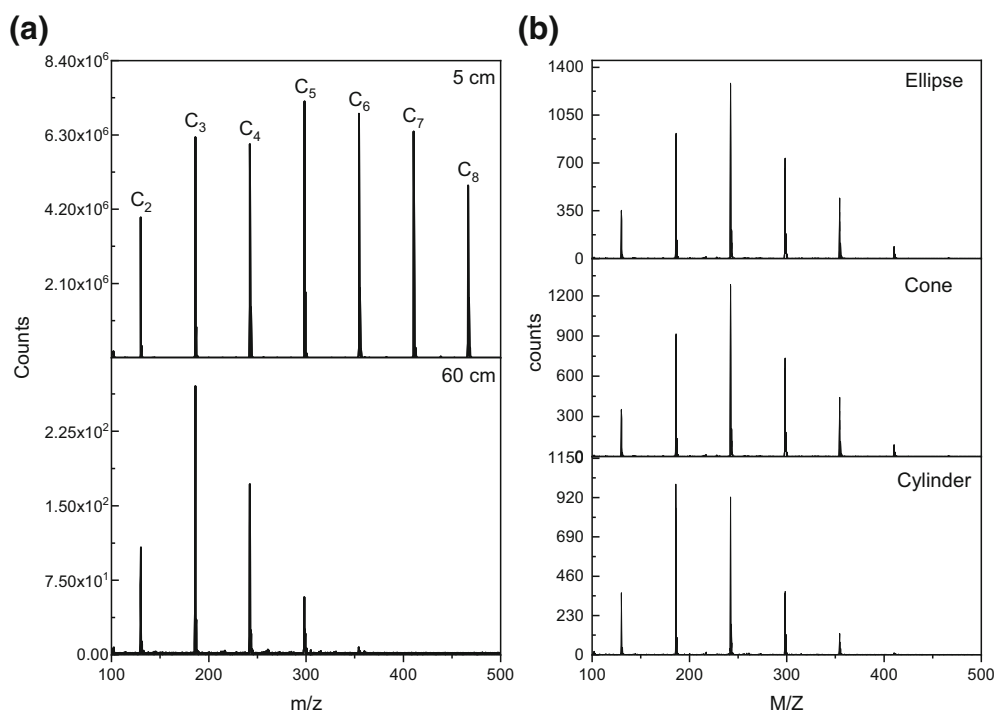
in Fig. S2 (supplemental information). For the MS results shown in Figure 3b, the nESI emitter was inserted into hole 1.

### Aperture Electrodes

The next set of experiments looked at focusing of ions through printed 2D apertures, building upon previous work in the group [21] in which electrosprayed ions were observed to undergo focusing by a factor of  $10\times$  through small apertures such as TEM grids. In these experiments, a  $5\text{-}\mu\text{m}$  O.D. nESI emitter was held 7.5 mm from the aperture, which in turn was held 7.5 mm from the IonCCD detector. The IonCCD was scanned over the ion cloud to observe focusing in both the vertical and horizontal directions.

First, a series of non-conductive apertures are considered. Shown in Figure 4 are the IonCCD images for the spray plume when using 3-mm, 9-mm, 12-mm, and 15-mm apertures. As the aperture size shrinks, so too does the size of the focused spot. All spots have FWHM values which are significantly smaller than is the aperture. The focusing achieved here is attributed to surface charging, viz. the buildup of charge on the aperture due to ion deposition.

After a critical amount of charge is deposited, ions are repelled from the surface towards the electrode center, where they form a collimated beam. Next, conductive apertures of the same sizes were explored. The data collected for a range of voltages and aperture sizes is given in Figure 5. It is



**Figure 3.** (a) Mass spectra showing profiles of sample consisting of a mixture of TAA salts. Top blue: Mass spectrum at 2 in. Bottom red: Mass spectrum at 60 cm. (b) Mass spectra showing profiles of a mixture of TAA salts with nESI in hole 1 of focusing electrodes placed at a distance of 60 cm. Top blue—ellipsoidal, middle red—Conical, bottom green—cylindrical. The nESI emitter was held at 3 kV while the focusing electrodes were held at 2 kV

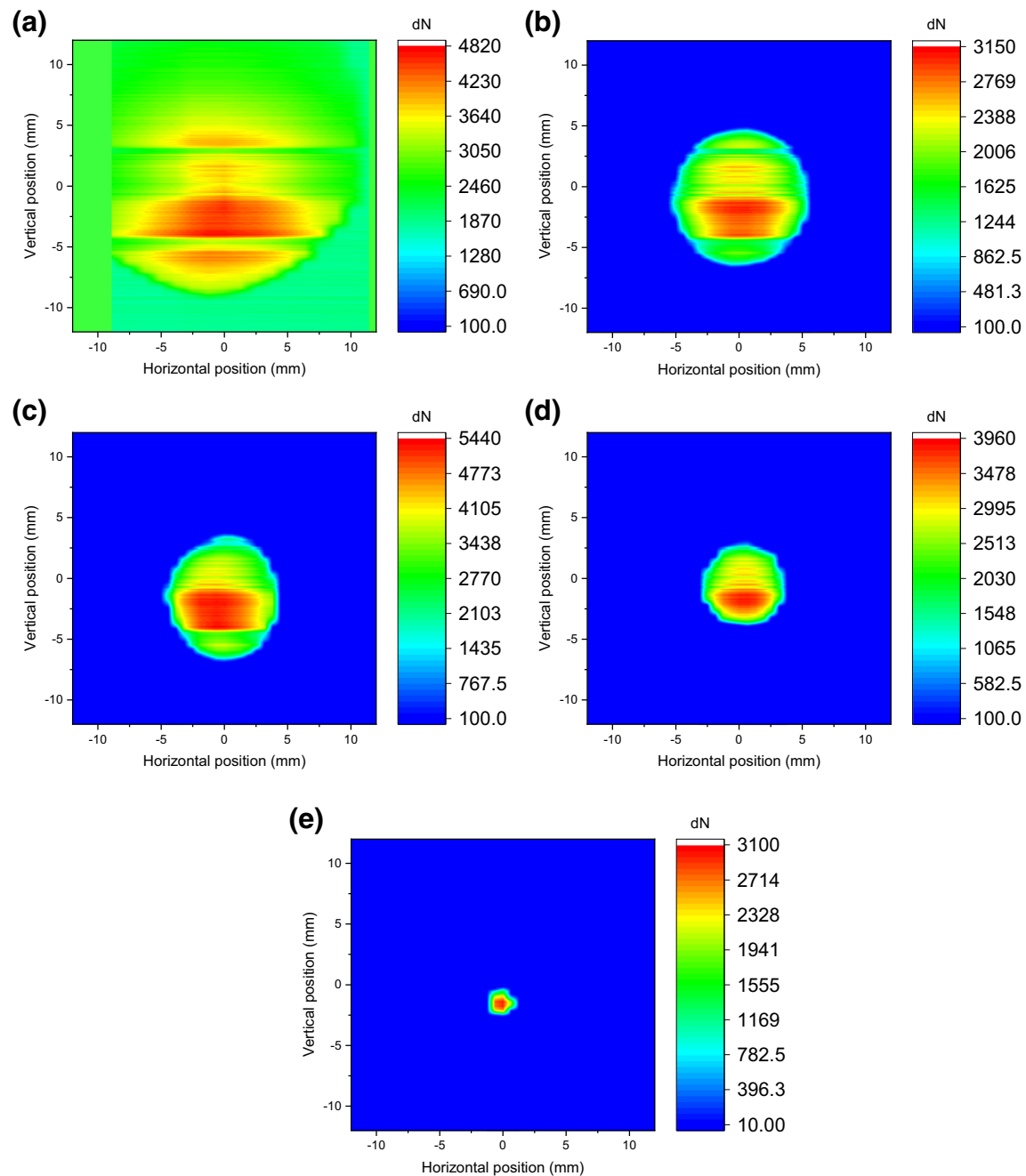


immediately apparent that, as the voltage on the aperture increases, the ion beam FWHM decreases. In addition, as the aperture size decreases the FWHM decreases at constant voltage. Finally, comparison of the 15-mm aperture data at 1 kV with 2 kV and 1.5 kV spray potentials shows that the beam FWHM decreases with increasing difference between aperture potential spray potential. The spatial irregularities in the IonCCD images for the apertures, both non-conductive and conductive, are attributed to the asymmetric nature of the nESI plume that is being focused (see Figure 4a). The regions of

irregular intensity are smoothed over as the microdroplets from the spray are reduced in size. For example, the conical electrodes, the cylindrical electrode IonCCD images show an irregular structure at 5 mm distance, but a relatively smooth structure at longer distances

### Complex Electrodes

Finally, to build upon the work using the simple geometries just described, focusing and transport in complex



**Figure 4.** Non-conductive apertures. (a) IonCCD intensity of nESI plume. Ion CCD images of beam focus through (b) 15 mm, (c) 12 mm, (d) 9 mm, and (e) 3-mm apertures. Note the differing color and axes scales for each figure

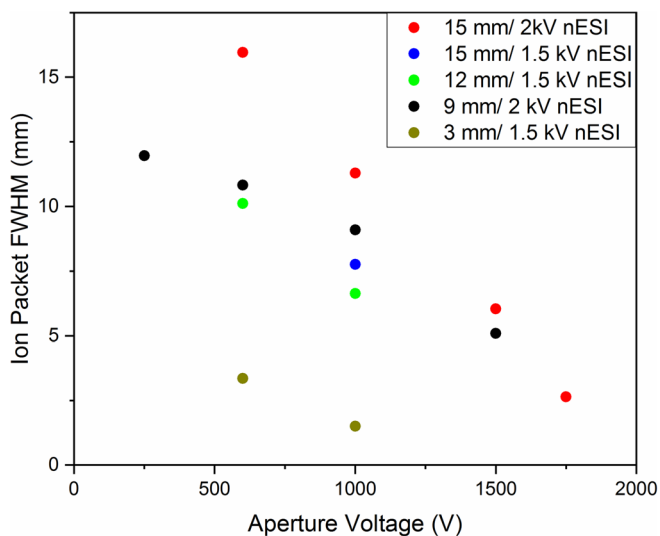


Figure 5. Summary of all conductive aperture ion beam data obtained from IonCCD images. For representative IonCCD images, see Fig. S3

electrodes was studied. Here, three electrode geometries were explored using the same six electrodes. The first was a curve, the second, a chicane, and the third, a straight path. The electrodes were arranged with the emitter approximately 5 mm into the first electrode and the IonCCD located 7.5 mm from the exit of the electrode. In these experiments, a mixture of four TAAs ( $C_3$ ,  $C_4$ ,  $C_6$ , and  $C_8$ ) was chosen for study. The emitter in all

cases was held at 6 kV, while the electrodes were floated with the first electrode at 3 kV or 4 kV, descending in either 500 V (for 3 kV) or 666 V (for 4 kV) steps.

As seen in Figure 6, for the curved electrode, the IonCCD data showed an asymmetrical spot, with higher intensity at higher voltage. Cuts through the collected data confirm that, as voltage is increased, the asymmetry also increases. The chicane electrode showed a similar, although less pronounced, asymmetry at high voltage. At lower voltage, the peak is largely symmetrical. Finally, the straight electrode shows a flat distribution at higher voltage, but at lower voltage, the intensity is mostly seen at the edge of the ion distribution. For the curved and the S-shaped electrodes, most of the ions are lost, perhaps due to the fact that they hit the walls of the device. The geometry of the electrodes results in an asymmetric electric field which in turn causes the asymmetry observed in the ionCCD images.

### SIMION Simulations

*Conical Section Electrodes* The cone, ellipsoidal, and cylindrical electrodes were simulated with an electrode potential of 3 kV, and an initial ion energy of 4.5 kV with an electrode, separated from the electrode exit, held at 0 V. The distance from the 0 V electrode to the electrode exit was 15 mm. The ion packet was placed at some distance in the electrode, but given a Gaussian distribution in the  $x$  and the  $y$  planes. The ions had

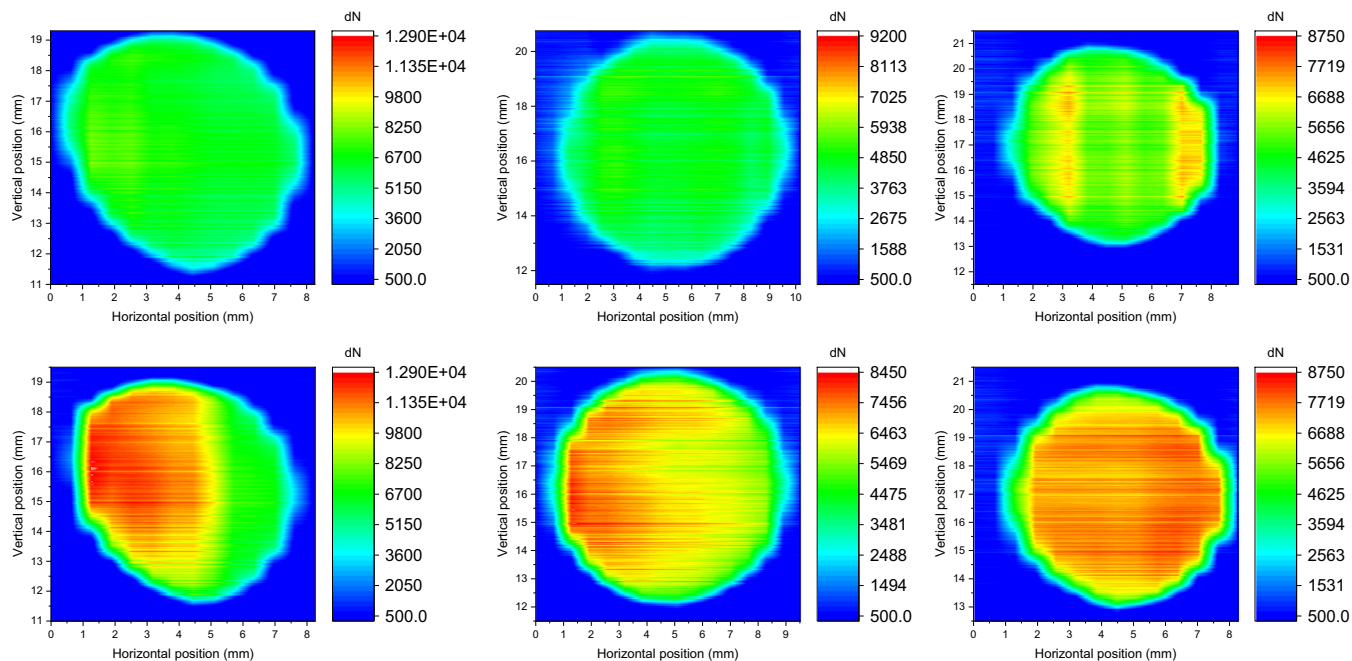


Figure 6. IonCCD images of ion beam focus through (left) curved complex electrode, (middle) chicane complex electrode, and (top) straight complex electrode. Top images correspond to initial float voltage of 3 kV, while bottom corresponds to initial float voltage of 4 kV

masses centered around  $m/z$  250. Representative traces are shown in Fig. S4.

SIMION simulations results for each electrode are shown in Figure 7. Note that, for each electrode type, the farther the emitter is from the electrode exit, the narrower the ion packet becomes. It is also clear that the ions do not spread after exiting the electrode, indicating that atmospheric collisions serve to maintain collimation of the beam when traveling outside the radial confining field. Intriguingly, the loss of ions with emitter distance is not replicated here, indicating that some other physics is likely at play. Still, the results of the simulations show qualitative agreement with the experimental results for the focusing behavior of the different electrodes, although focusing differences between electrodes are not well captured. While only bare ions are considered in these simulations, it is likely that charged droplets from the emitter are also focused in the experiment, which could have an impact on the agreement of these results with experiment.

*Apertures* Representative simulations of the 15-mm conductive aperture are shown in Fig. S5 (supplementary information). The parameters for ion creation were similar to those for

the conic section electrodes, except for initial kinetic energy, which was held at either 2 kV or 1.5 kV, taken to be the maximum possible kinetic energy of an ion produced from the emitter. The effect of kinetic energy on the SIMION simulations is shown in supplemental Fig. S5A. The potential on the aperture was varied to match the experimental parameters which were probed. Here, it was found that modeling the nESI emitter was necessary to obtain the desired physics seen in the experiment. In all cases, the ion behavior observed matched with the experimental data, indicating that the voltage difference between the emitter and aperture is the primary determinant of ion focusing, with smaller differences giving better focusing.

*Complex Electrodes* Simulations of the complex geometry electrodes are shown in Fig. S6 (supplementary information). In these experiments, the ion kinetic energy was held at 6 kV, while the electrode potentials were modeled after the 3-kV case experiments. The initial ion kinetic energy has little effect on the observed trajectories, as seen in Fig. S7. It is immediately apparent that the simulations match poorly with experimental data, although the straight electrode shows the best agreement.

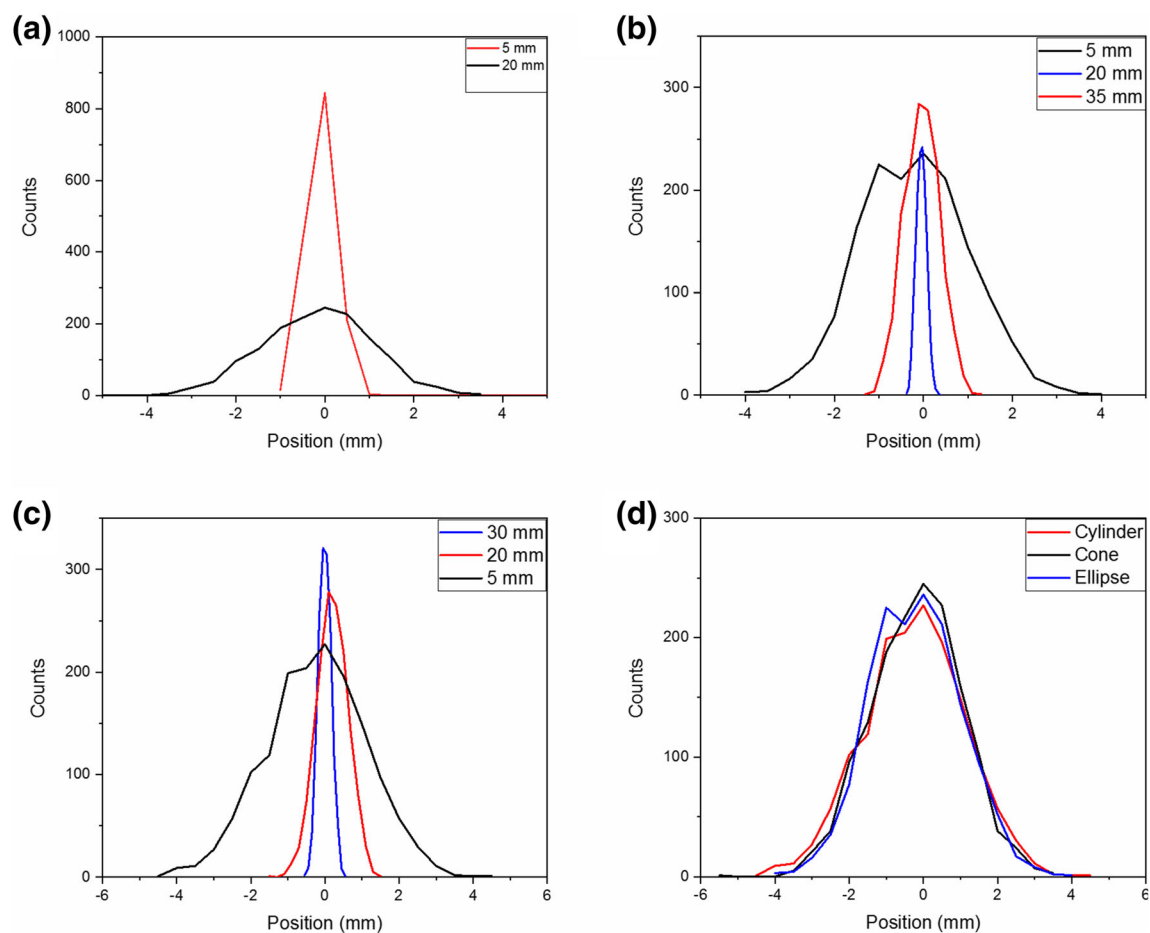


Figure 7. simulations of ion packet focus from (a) conical, (b) cylindrical, and (c) ellipsoidal electrodes. (d) Comparison of the 5-mm electrode spots



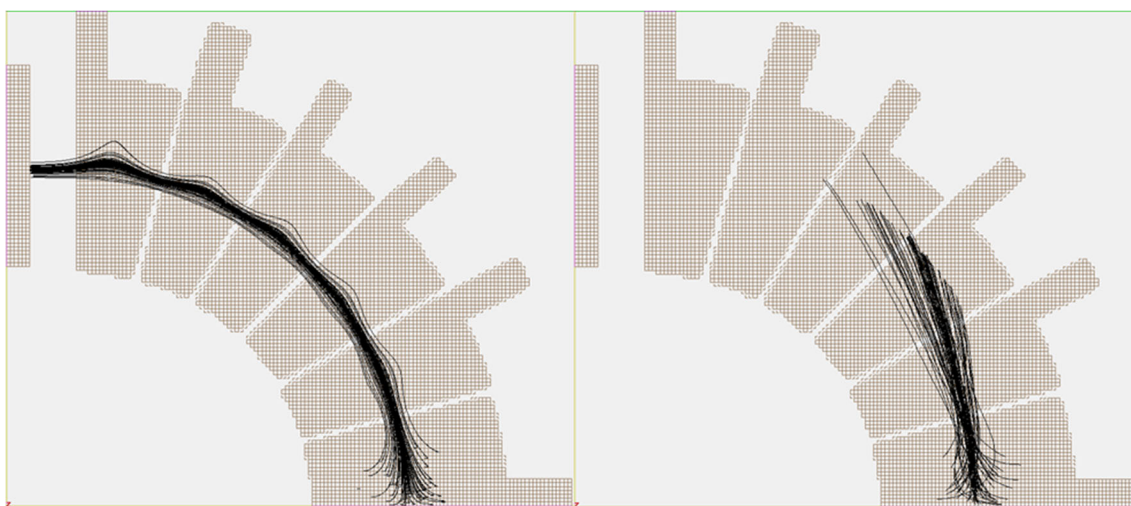
Specifically, the asymmetry of the ion packet is well reproduced. The focusing is grossly overestimated for the other electrodes, however. Note that the ion losses from the experiment are also not well reproduced.

### *Rationalization of Results: Focusing Mechanism*

From the differences between the experimental measurements and simulations, it is clear that the observed ion focusing and transport results from the interplay of a number of different variables and that these are not fully captured by the available simulations. Certain things, however, are clear: (i) In contrast to vacuum conditions, ions in the open air are subjected to collisional forces from background gas molecules. At standard temperature and pressure, an ion will undergo a collision on the order of  $10^{10}$  times per second with a background gas molecule. This results in fast momentum transfer from the ion to the neutral background molecules, which slows the ion (collisional cooling). Although the ions may have initial energies on the order of 1 keV, and background molecules may have energies of only a few meV, the frequency of collisions is such that ion trajectories may be significantly altered (collisional broadening). (ii) A related process which will also influence focusing is the desolvation of ions as they travel in the open air or through a device. Ions are born from charged microdroplets which undergo evaporation more or less quickly depending on the solvent, to give bare ions. The shrinking droplets also will have less momentum, even at the same energy due to the reduction in mass, further influencing the collision dynamics. While this dynamic process cannot be modeled by SIMION, it should not be overlooked as a factor in the behavior

observed here. (iii) The electric field plays a role, specifically, the field interacts with the ion cloud to change the ion position in space by repelling or attracting charged droplets and ions. For the apertures and conic section electrodes used here, the electric field is symmetric around the center of the device. Thus, ions are “channeled” to this region, which reorients their velocities resulting in collimation of the ion beam. This is best exemplified by the changing of the ion packet size with lower emitter voltage in the case of the 15-mm conductive aperture. The ion kinetic energy is greatly influenced by the electric potentials of the aperture and the nESI emitter, with the larger voltage difference giving rise to the highest energy ions. Lower kinetic energy means that the ions must go to an area with lower electric field to pass through the aperture, which explains, in part, the increased focus. (iv) This collimation might be aided by the collisions of background gas molecules with the ion cloud, as this constrains the ions from spreading due to space charge between ions.

The experimental fact is that a tight focus can be maintained over significant distance, even when ions have exited the electrode. In the case of the asymmetric electrodes, the ions still follow the path of the lowest electric field, although this results in the asymmetry observed in the ion cloud. The mass spectral results of the conic section electrodes, which showed increased signal from heavy ions at long distances, indicate that ion transmission is influenced by the electrodes. It is postulated that the increased energy of the ions as they leave the electrode gives higher kinetic energies compared to nESI alone, thus increasing the chance of transmission of such ions. It is also postulated that the coupling of the electric field and collision effects gives rise to focusing. The fact of focusing is evident from the experimental data and from some of the simulations, for example that shown in Figure 8. Here, a simulation of ion



**Figure 8.** Simulations of ions traveling through the curved electrode in the presence of atmospheric gas (left) and in vacuum (right). The direction of ion travel is from the bottom right opening of the electrodes. Note that ions are not transmitted to the exit when collisions are not present

cloud trajectory is shown for ambient pressure and vacuum conditions. The ambient pressure scenario gives rise to ion transport through the device, while in vacuum, the ions are relatively unaffected by the changing electrode potentials and collide with the walls of the device instead of passing through. This implies that collisions result in a lowering of ion energy to match the changing electric field in the device. These observations suggest that high pressures, while requiring different device design considerations, should be viewed not as a hindrance to ion transport, but instead as a potentially useful force. It is also clear that the focusing effect is incompletely understood.

## Conclusions

In this study, focusing of nESI-generated ions in air was achieved by using only DC potentials on various designs of 3D-printed electrodes. The electric field plays a role in focusing and transmission of ions to the mass spectrometer, but collisions with the background gas (air in this case) are also crucial to the observed focusing. Mass spectral data shows that these devices are also capable of increasing the signal of high mass species at large distances relative to nESI alone, indicating improved ion transmission. The simplicity and ease of construction of these devices with 3D-printing is an additional advantage. Finally, simulations were performed to corroborate findings and optimize how ions are transmitted in the open air and at atmospheric pressure interface of the mass spectrometer. Simulation results showed qualitative agreement in many cases, although the curved electrodes gave poor agreement. One obvious source of error is that the simulations only consider desolvated ions, instead of charged microdroplets.

## Acknowledgements

This work was supported by Agilent Technologies Inc. through gift #4212. We thank Pei Su and Julia Laskin for assistance with the IonCCD measurements.

## References

1. Fenn, J.B., Mann, M., Meng, C.K., Wong, S.F., Whitehouse, C.M.: Electrospray ionization-principles and practice. *Mass Spectrom. Rev.* **9**(1), 37–70 (1990)
2. Takats, Z., Wiseman, J.M., Gologan, B., Cooks, R.G.: Mass spectrometry sampling under ambient conditions with desorption electrospray ionization. *Science*. **306**(5695), 471–473 (2004)
3. Wang, H., Liu, J.J., Cooks, R.G., Ouyang, Z.: Paper spray for direct analysis of complex mixtures using mass spectrometry. *Angew. Chem. Int. Ed.* **49**(5), 877–880 (2010)
4. Harris, G.A., Galhena, A.S., Fernandez, F.M.: Ambient sampling/ionization mass spectrometry: applications and current trends. *Anal. Chem.* **83**(12), 4508–4538 (2011)
5. Stopka, S.A., Samarah, L.Z., Shaw, J.B., Liyu, A.V., Velickovic, D., Agtuca, B.J., Kukolj, C., Koppenaal, D.W., Stacey, G., Pasa-Tolic, L., Anderton, C.R., Vertes, A.: Ambient metabolic profiling and imaging of biological samples with ultrahigh molecular resolution using laser ablation electrospray ionization 21 tesla FTICR mass spectrometry. *Anal. Chem.* **91**(8), 5028–5035 (2019)
6. Alberici, R.M., Simas, R.C., Sanvido, G.B., Romao, W., Lalli, P.M., Benassi, M., Cunha, I.B.S., Eberlin, M.N.: Ambient mass spectrometry: bringing MS into the "real world". *Anal. Bioanal. Chem.* **398**(1), 265–294 (2010)
7. Page, J.S., Kelly, R.T., Tang, K., Smith, R.D.: Ionization and transmission efficiency in an electrospray ionization-mass spectrometry interface. *J. Am. Soc. Mass Spectrom.* **18**(9), 1582–1590 (2007)
8. Cox, J.T., Marginean, I., Smith, R.D., Tang, K.Q.: On the ionization and ion transmission efficiencies of different ESI-MS interfaces. *J. Am. Soc. Mass Spectrom.* **26**(1), 55–62 (2015)
9. Cech, N.B., Enke, C.G.: Practical implications of some recent studies in electrospray ionization fundamentals. *Mass Spectrom. Rev.* **20**(6), 362–387 (2001)
10. Kelly, R.T., Tolmachev, A.V., Page, J.S., Tang, K.Q., Smith, R.D.: The ion funnel: theory, implementations, and applications. *Mass Spectrom. Rev.* **29**(2), 294–312 (2010)
11. Amsden, J.J., Gehm, M.E., Russell, Z.E., Chen, E.X., Di Dona, S.T., Wolter, S.D., Danell, R.M., Kibelka, G., Parker, C.B., Stoner, B.R., Brady, D.J., Glass, J.T.: Coded apertures in mass spectrometry. *Annu. Rev. Anal. Chem.* **10**, 141–156 (2017)
12. Janulyte, A., Zerega, Y., Andre, J., Brkic, B., Taylor, S.: Performance assessment of a portable mass spectrometer using a linear ion trap operated in non-scanning mode. *Anal. Chem.* **88**(12), 2407–2415 (2016)
13. Badu-Tawiah, A.K., Wu, C.P., Cooks, R.G.: Ambient ion soft landing. *Anal. Chem.* **83**(7), 2648–2654 (2011)
14. Saf, R., Goriup, M., Steindl, T., Hamedinger, T.E., Sandholzer, D., Hayn, G.: Thin organic films by atmospheric-pressure ion deposition. *Nat. Mater.* **3**(5), 323–329 (2004)
15. Li, A.Y., Luo, Q.J., Park, S.J., Cooks, R.G.: Synthesis and catalytic reactions of nanoparticles formed by electrospray ionization of coinage metals. *Angew. Chem. Int. Ed.* **53**(12), 3147–3150 (2014)
16. Baird, Z., Peng, W.P., Cooks, R.G.: Ion transport and focal properties of an ellipsoidal electrode operated at atmospheric pressure. *Int. J. Mass Spectrom.* **330**, 277–284 (2012)
17. Baird, Z., Wei, P., Cooks, R.G.: Ion creation, ion focusing, ion/molecule reactions, ion separation, and ion detection in the open air in a small plastic device. *Analyst*. **140**(3), 696–700 (2015)
18. Foo, C., Lim, H. N., Mahdi, M. A., HaniffWahid, M., Huang, N. M.: Three-dimensional printed electrode and its novel applications in electronic devices. *Sci Rep-Uk.* **8** (2018)
19. Hadjar, O., Schlatholter, T., Davila, S., Catledge, S.A., Kuhn, K., Kassan, S., Kibelka, G., Cameron, C., Verbeck, G.F.: IonCCD detector for miniature sector-field mass spectrometer: investigation of peak shape and detector surface artifacts induced by keV ion detection. *J. Am. Soc. Mass Spectrom.* **22**(10), 1872–1884 (2011)
20. Appelhans, A.D., Dahl, D.A.: SIMION ion optics simulations at atmospheric pressure. *Int. J. Mass Spectrom.* **244**(1), 1–14 (2005)
21. Li, A.Y., Baird, Z., Bag, S., Sarkar, D., Prabhath, A., Pradeep, T., Cooks, R.G.: Using ambient ion beams to write nanostructured patterns for surface enhanced Raman spectroscopy. *Angew. Chem. Int. Ed.* **53**(46), 12528–12531 (2014)